# CT Thermometry for Cone-beam CT Guided Ablation

Zachary DeStefano[a], Nadine Abi-Jaoudeh[b], Ming Li[c], Bradford J Wood[b], Ronald M Summers[a], Jianhua Yao[a]

[a]Clinical Image Processing Services, Radiology and Imaging Sciences, Clinical Center, National Institutes of Health, Bethesda, MD 20892
[b]Interventional Radiology, Radiology and Imaging Sciences, Clinical Center, National Institutes of Health, Bethesda, MD 20892
[c]National Heart, Lung and Blood Institute, National Institutes of Health, Bethesda, MD, USA

## ABSTRACT

Monitoring temperature during a cone-beam CT (CBCT) guided ablation procedure is important for prevention of over-treatment and under-treatment. In order to accomplish ideal temperature monitoring, a thermometry map must be generated. Previously, this was attempted using CBCT scans of a pig shoulder undergoing ablation.[1] We are extending this work by using CBCT scans of real patients and incorporating more processing steps. We register the scans before comparing them due to the movement and deformation of organs. We then automatically locate the needle tip and the ablation zone. We employ a robust change metric due to image noise and artifacts. This change metric takes windows around each pixel and uses an equation inspired by Time Delay Analysis to calculate the error between windows with the assumption that there is an ideal spatial offset. Once the change map is generated, we correlate change data with measured temperature data at the key points in the region. This allows us to transform our change map into a thermal map. This thermal map is then able to provide an estimate as to the size and temperature of the ablation zone. We evaluated our procedure on a data set of 12 patients who had a total of 24 ablation procedures performed. We were able to generate reasonable thermal maps with varying degrees of accuracy. The average error ranged from 2.7 to 16.2 degrees Celsius. In addition to providing estimates of the size of the ablation zone for surgical guidance, 3D visualizations of the ablation zone and needle are also produced.

**Keywords:** Cone-beam CT, CBCT, Thermometry, Radiofrequency Ablation, Time Delay Analysis

## 1. INTRODUCTION

Radiofrequency ablation (RFA) has become a common interventional procedure for treating cancerous tumors in various parts of the body.[2] During the operation, a thin needle is inserted into the body and guided toward the tumor. Once it reaches the tumor, high-frequency energy passes through the needle which causes the surrounding tissue to increase in temperature. This heat kills the nearby cells including the tumor.

C-arm Cone-beam CT (CBCT) is an imaging modality that has been adopted for a variety of purposes,[3] including guidance during RFA. Unlike traditional CT scans, the source and detector with CBCT are easily shifted to various locations. Once the source and detector are in place, they rotate around a fixed point of interest. This allows volumetric data to be acquired quickly and easily during interventional procedures without the need for patient transportation. This occurs because the data is acquired via only a single rotation of the scanner.

Even though CBCT provides much useful information, it is still difficult to determine how much tissue has been affected by the procedure. Specifically, we need to know the temperature changes that have occurred in the tissue. We want to make sure only the cancerous tissue has been heated and not the healthy tissue. Ideally, each of the CBCT voxels would also have a temperature reading. We would then be able to superimpose the thermal volume on the CBCT scan and quickly find out which tissue has been affected.

This possibility has been explored in the past[1] but only for phantoms. We decided to extend the work to real patients and incorporate more processing steps to enhance the thermal maps. For this work, we had a data

set of CBCT scans taken during RFA procedures. With each procedure, there was a baseline CBCT scan taken after the ablation needle was inserted but before it was heated. There were then 1-4 comparison scans taken as the needle was heated and cooled. We processed each of the comparison scans and attempted to generate a thermal map by comparing them to the baseline scan.

## 2. RELATED WORK

### 2.1 CT Thermometry

CT Thermometry has been explored since the late 1970's with some success.[4] Many of the attempts focused on correlating individual HU unit values with temperature. For our purposes this would not work because these values can be heavily influenced by image noise and metal artifacts. An additional issue with previous attempts is that they used stationary phantoms. We decided to attempt CT Thermometry on real patients meaning that the movement and deformation of organs had to be taken into account. Due to these issues, we employed additional processing steps as well as a more robust change metric than raw difference.

### 2.2 Image Registration

Medical Image Registration has been researched extensively.[5,6] For our purposes, we needed to align temporal sequences of CBCT scans. In particular, we performed an affine registration in order to account for movement of the organs during the ablation procedure. The organs can deform thus we also incorporated non-rigid registration. There is now an open source tool known as NiftyReg[7,8] that was able to perform both the affine[7] and deformable[8] registration.

### 2.3 Wronskian Change Metric

Previously, the Wronskian Change Detector[9] was proposed as a metric that would be robust to noise.[1] This particular change detector has been shown to perform well for classification problems[9–12] in image analysis. The formula however computes the ratios between intensity values. Because the relationship between HU unit value and temperature is roughly linear,[4] we need a function that increases linearly as the change in HU unit increases. Additionally, when computing the Wronskian, the location of the pixels is quite important, meaning it is not robust to motion artifacts. Due to these issues, we decided not to use the Wronskian Change Detector.

### 2.4 Time Delay Analysis

It is a common problem in signal processing to have two nearly identical signals that are offset by a delay. In order to calculate the most likely delay, cross-correlations are used.[13] The cross-correlation of two real-valued discrete signals $f$ and $g$ is defined as follows:

$$(f \star g)[n] = \sum_{m=-\infty}^{\infty} f[m]g[m+n]$$

The most likely delay $t_{delay}$ occurs when the correlation is the highest thus

$$t_{delay} = \arg\max_{t}(f \star g)[t]$$

For our purposes, we will take two square small images $U$ and $V$ and interpret them as periodic 2D signals that continuously repeat horizontally and vertically. Extrapolating from time delay analysis, the ideal spatial offset between the images occurs when the correlation is highest. Thus our ideal offset $(r, c)$ is as follows:

$$(r, c)_{offset} = \arg\max_{r,c} \sum_{l=0}^{n-1} \sum_{k=0}^{n-1} U_{k+r,l+c} \cdot V_{k,l}$$

The offset values found here are equivalent to the ones that are found in the Spatial Offset RMSE method.

## 3. PIPELINE

In order to generate thermal maps from the comparison CBCT scans, we did the processing only in the region where the ablation occurred. This is because the relationship between Hounsfeld Units (HU) in CT scans and temperature varies depending on which organ is being affected.[4] Thus our maps would be inaccurate for other tissue. Because the needle has distinct HU values from tissue and the ablation occurred at the tip of the needle, we were able to attempt automation of finding this region.

There is strong evidence that the relationship between HU unit and temperature is linear[4] thus we correlated change in HU with change in temperature. Because of CBCT scan artifacts and noise, we had to use a different change metric than simple difference but one that still behaved linearly as HU units changed. Ultimately, we incorporate two change metrics into our pipeline that fit the criteria, Filtered Difference and Spatial Offset RMSE.

The Filtered Difference method involves filtering both scans with an averaging filter and then obtaining the difference image. The Spatial Offset RMSE method involves taking a window around a pixel in both scans and computing the minimum RMSE of the values in the windows assuming there is a spatial offset between them. The Spatial Offset RMSE method is more computationally intensive than the Filtered Difference method but it produces a much smoother change map. We thus use the Filtered Difference to give us an estimate of the thermal map in order to verify our choice of region. We then use the Spatial Offset RMSE to compute the estimate of the thermal map.

For each comparison scan, a corresponding thermal map was generated via the following procedure:

1. Register the comparison scan to the baseline scan
2. Use Connected Component Analysis and Principal Component Analysis (PCA) to detect the Needle and Thermocouple tips
3. Use the result to obtain the ROI where the ablation occurred. If that fails, manually input the ROI.
4. Filter the ROI in the baseline and comparison scans with an averaging filter, and calculate the difference
5. Use the result to locate where the ablation likely occurred
6. Calculate the Spatial Offset RMSE value for the ROI
7. Correlate Spatial Offset RMSE values at the temperature zones with the measured temperature data there.
8. Use the regression model from the correlation calculated to generate a thermal map for the ROI

### 3.1 Image Registration

For the registration step, the comparison scan volume was registered to the baseline scan volume using the software package NiftyReg. We used the **reg aladin** command to perform an affine registration[7] in order to account for movement of the organs between different scans. We then used the **reg f3d** command to perform non-rigid registration[8] in order to align the organs in such a way that accounted for changes in their shape between scans. Figure 1 shows an example of image slices before and after registration.

### 3.2 ROI Detection

The HU values for the needle and thermocouple are significantly higher than the values for normal tissue. Thus after thresholding the values in the CBCT scan high enough, the points remaining are the ones in the needle and thermocouple. Doing connected component analysis with **bwconncomp**[14] in Matlab let us find the clusters which contain the needles and thermocouples. For each cluster, **pca**[15] in Matlab was done to find the needle vector and endpoints. Figure 2 shows the result after performing this procedure for one of our patients.

We now have a series of endpoints and for each one, the region around it is a potential ROI. For each potential ROI, we can verify it by inspecting the CBCT scan in that region and qualitatively assessing if the ablation occurred. Additionally, the Filtered Difference method can be used to approximate the thermal map, thus indicating if the ablation has occurred. If our method fails to find the ROI, then we use those techniques on the whole CBCT scan and manually find and input the box around the ablation zone.

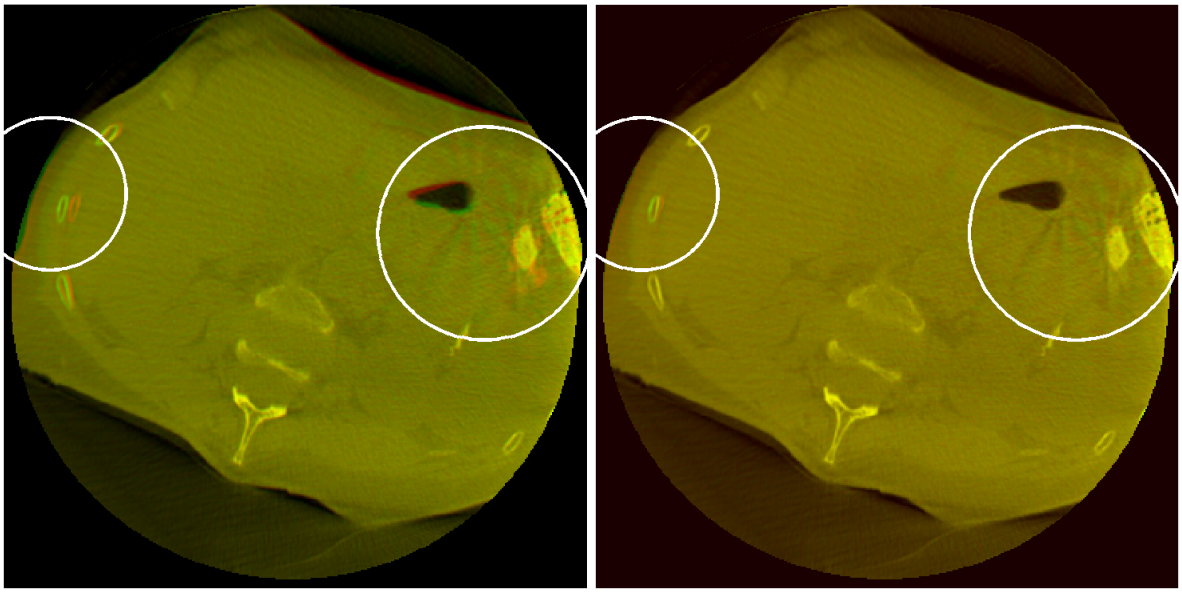

(a) Before Registration (b) After Registration

Figure 1: Baseline (green channel) and Comparison (red channel) Image superimposed in one image before and after registration

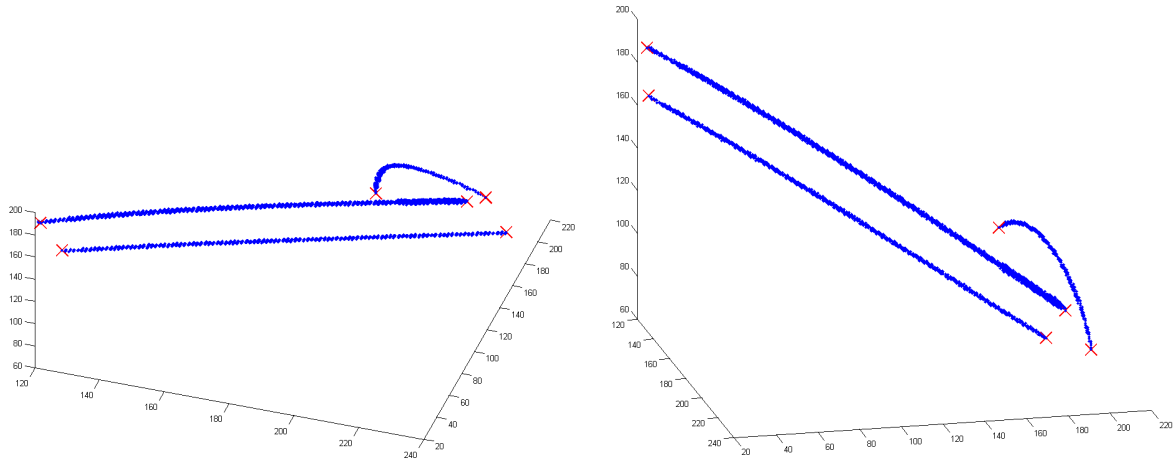

Figure 2: Needles and Thermocouple (blue) and their endpoints (red) detected using PCA

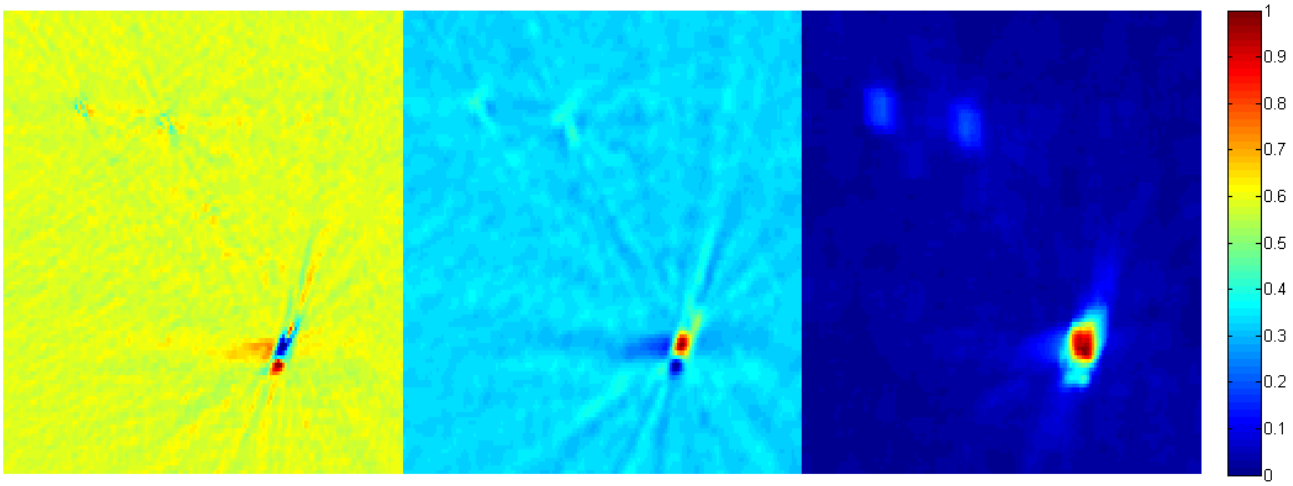


Figure 3: Results of different change metrics in the ROI. Raw subtraction (left), Filtered Difference (center), and Spatial Offset RMSE (right). Each image is normalized in order to show how the thermal map would appear

### 3.3 Change Detection

These images have a low signal to noise ratio as well as beam hardening artifacts. We thus decided to use a window around each pixel in order to obtain a more robust change value. Initially we calculated the mean difference between the baseline image window and the comparison image window and used that as the value of the pixel in the result image. This is equivalent to performing a convolution on both images with an averaging filter and then taking the difference between the filtered images. The result images were used to provide an estimate of how the thermal map will appear. They are still too noisy to be used for the thermal map though.

In order to find a better result image, for each pixel, we calculated the minimum RMSE between the baseline and comparison windows assuming that there is a spatial offset between them. For each pixel, let $U$ be the $n$ by $n$ window around it in the baseline image and let $V$ be the $n$ by $n$ window around it in the comparison image. We made the matrix $U'$ which is $U$ repeated in the following manner:

$$\forall(k, l, i \in Z)\ \ U'_{k+i\cdot n, l+i\cdot n} = U_{k,l}$$

Afterward the following was calculated and the value was stored as the pixel value in the result image:

$$\min_{r,c} \sqrt{\frac{1}{n^2} \sum_{l=0}^{n-1} \sum_{k=0}^{n-1} (U'_{k+r,l+c} - V_{k,l})^2}$$

Figure 3 shows the result image after applying the methods to an example slice in the baseline and comparison CBCT scan. As can be observed, raw subtraction gives us the noisiest result hence the need for a better metric. Filtered Difference gives us a much better result but there is still much noise and many artifacts. Spatial Offset RMSE gives us the smoothest map.

### 3.4 Regression

After generating the Spatial Offset RMSE result image, we find the coordinates where the measured temperature zones are located. Each zone center and its measured temperature are manually inputted into the program. The points a small neighborhood around the zone center are all used as result image values. We correlate the result image values with the measured temperature changes using linear regression. We then take the regression equation calculated and apply it to the result image to generate a thermal map. Figure 4 shows the plot of Spatial Offset RMSE versus Temperature Change as well as the regression curve calculated from it. Figure 5 shows the resulting thermal map.

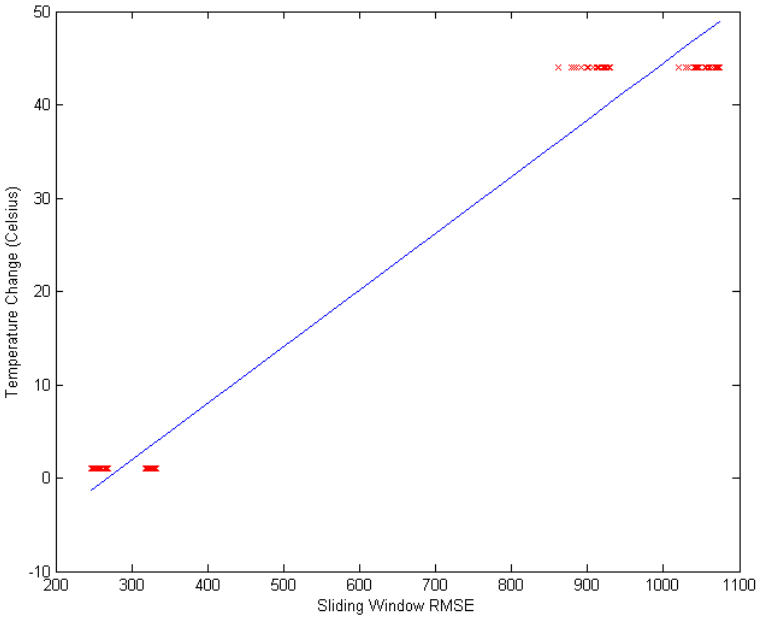

Figure 4: Regression Curve Calculated

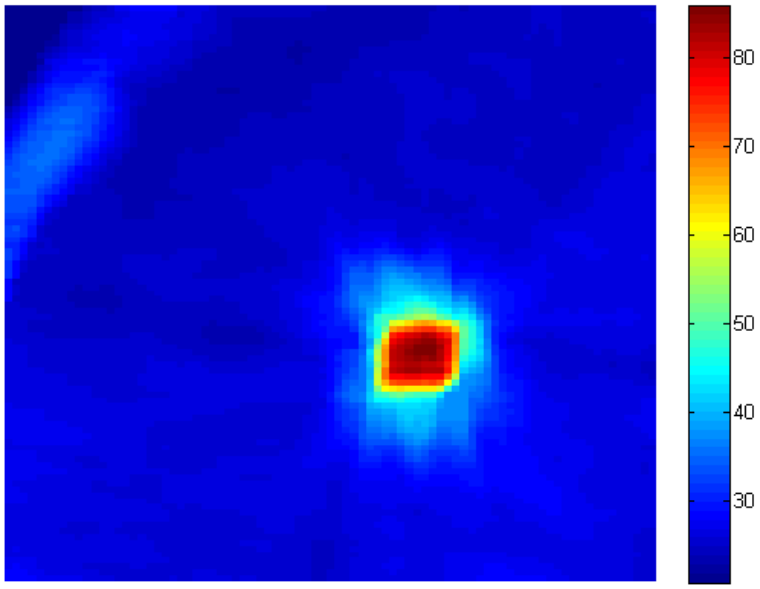

Figure 5: Thermal Map generated from Regression curve

## 4. RESULTS

We used a data set of CBCT scans taken for 13 patients whose procedures were performed between September 2013 and June 2015. For each patient, there were between 1 and 4 ablations done. With each ablation, a baseline scan was taken followed by 1-4 comparison scans at different time points. Each of these time points had the ablation needle at different temperatures. We generated a thermal map at each of these time points in order to estimate the amount of tissue affected.

### 4.1 Finding Error Rates

We decided to take the thermal maps generated from regression and see the average temperature in the zones that we were testing. We then did an RMSE of those temperatures with the measured temperatures. We divided this RMSE by the temperature range in order to obtain an error ratio. The results are in table 1. In the table, temperatures are in Celsius and *Temps (From Regression)* is the average temperature in the neighborhood around the needle or thermocouple (with radius specified by *Neighborhood Radius*) in the thermal map calculated from regression. Our error rate ranged from 8-22% and the error amount ranged range 2.7 to 16.2 degrees Celsius.

| Pt Num | 4 | 5 | 5 | 6 | 8 | 9 |
|---|---|---|---|---|---|---|
| Procedure Num | 1 | 1 | 3 | 1 | 1 | 1 |
| Pt Sex | M | M | M | F | F | F |
| Pt Age | 54 | 48 | 48 | 65 | 59 | 61 |
| | | | | | | |
| Baseline Temps | 36/36 | 35/35 | 38/36 | 31/31/30 | 36/37 | 37/37 |
| Pixel size (mm) | 0.9823 | 0.9823 | 0.9823 | 0.9823 | 0.6549 | 0.6549 |
| Neighborhood Radius (mm) | 1.9646 | 1.9646 | 1.9646 | 1.9646 | 1.3098 | 1.3098 |
| | | | | | | |
| Comparison 1 | | | | | | |
| Temps (Given) | 64/56 | 58/38 | 48/83 | 132/124/45 | 100/37 | 145/42 |
| Temps (From Regression) | 67.2/59.6 | 64.2/45.4 | 50.9/62.2 | 128.4/108.9/81.0 | 111.0/36.6 | 142.6/56.5 |
| Time Since Baseline (min) | 14 | 10 | 10 | 7 | 5 | 55 |
| | | | | | | |
| Comparison 2 | | | | | | |
| Temps (Given) | 67/57 | 66/58 | 52/95 | 126/107/98 | 52/38 | 47/37 |
| Temps (From Regression) | 65.5/59.2 | 66.0/46 | 66.8/94.7 | 126.7/110.0/103.1 | 65.2/36.5 | 50.7/55.6 |
| Time Since Baseline (min) | 70 | 22 | 23 | 13 | 13 | 62 |
| | | | | | | |
| Given & Regression Temp RMSE | 2.752 | 7.7 | 12.847 | 16.189 | 8.626 | 11.997 |
| Error Ratio | 8.8774E-2 | 0.2484 | 0.2177 | 0.1587 | 0.2396 | 0.1110 |

### 4.2 Approximating Ablation Zone Area

After generating a thermal map, we identified the point with the highest temperature as being the likely center of ablation. We then made a graph showing the average temperature in a region around that point as a function of the radius of the region. We can potentially use the values of the function to approximate the radius of the ablation zone. Once the average is below a certain fixed temperature or below a certain percentage of the peak, we are outside the ablation zone. Figure 6 shows these values for various patients in our study.

### 4.3 3D Visualization of Ablation Zone

We were able to produce a 3D visualization of the needle and the ablation zone. We thresholded the values of the 3D Thermal Map generated which produced a binarized 3D volume. We also thresholded the values of the original CBCT scan in order to produce a binarized 3D volume showing only the needle. With both volumes, we ran a surface generation algorithm using ITK-SNAP.[16] This created two 3D meshes. We superimposed them in 3D Slicer[17] to show the needle and ablation zone together. Figure 7 displays the result.

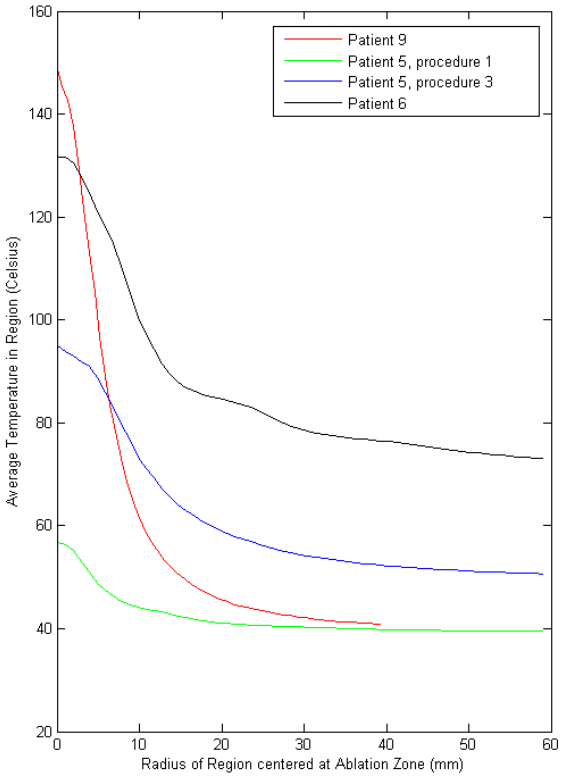


Figure 6: Graph of radius vs mean temperature

## 5. CONCLUSIONS

The processing steps we performed seem to be good initial steps toward incorporating CT Thermometry in clinical practice. Affine and Deformable Registration aligned the CBCT scans allowing us a much more accurate change map. Needle Detection provided a quick way of finding the ROI. The change metric we used provided smooth change maps that were able to generate reasonable thermal maps.

For some of the patients, these thermal maps were quite accurate while for others the error was higher. The higher error was the result of a high residual value in the linear regression. This was likely caused by image noise or registration error. In the cases where the error was low, the thermal maps have the potential to be quite useful during ablation procedures. They may be used to approximate the size of the ablation zone. Additionally, there is the potential to generate a 3D visual representation of the ablation zone.

## 6. FUTURE WORK

### 6.1 Metal Deletion Technique

There are a myriad of medical image filtering techniques that have been developed over the years. With regards to the metal artifacts in CT scans, a technique known as the Metal Deletion Technique[18] has developed which has shown to be quite effective. It reduces the artifacts quite well and has a relative low error in HU relative to the original image. In the future, we hope to incorporate this technique into the initial processing steps in order to produce an even smoother change map.

### 6.2 Further Testing

We hope these methods will continue to be tested and eventually incorporated into clinical practice. This will require testing on a lot more CBCT scans. Additionally, we will need a data set where multiple imaging modalities were employed. That way we can test our thermal map against one generated by a modality that is known to generate accurate thermal maps.

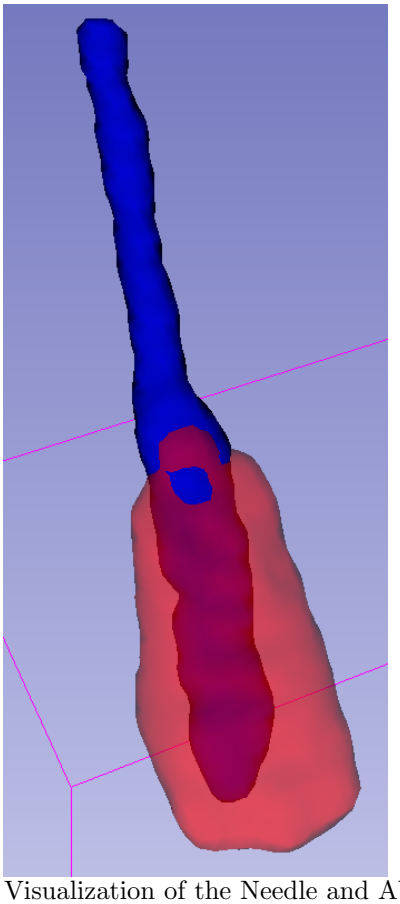

Figure 7: 3D Visualization of the Needle and Ablation Zone

### 6.3 Improve Running Time

Most steps in the pipeline currently take less than 30 seconds so applying them in clinical practice is possible. The registration step however takes 1-6 hours. This will need to be cut down if we are to use the registration step in clinical practice. We will either need to use a different registration algorithm or change the parameters of our current one to improve its running time. If the registration step cannot be done efficiently, then we may need to adjust our change metrics to be more tolerant of registration errors.

## ACKNOWLEDGMENTS

This project was a collaboration between the Clinical Image Processing Service (CIPS) and Interventional Radiology (IR) in the department of Radiology and Imaging Sciences at the National Institutes of Health Clinical Center. Thank you to the non-authors in CIPS who provided valuable guidance and insights, especially Holger Roth and Nathan Lay. Thank you to those in IR who helped acquire the patient data. Much of the analysis was done as an internship project during Summer 2015. The internship was funded by an NIH Intramural Research Training Award (IRTA) grant.

## REFERENCES

1. M. Li, N. Abi-Jaoudeh, A. Kapoor, S. Kadoury, S. Xu, N. Noordhoek, A. Radaelli, B. Carelsen, and B. J. Wood, "Towards cone-beam ct thermometry," *Proc. SPIE 8671* , March 2013.
2. Mayo Clinic Staff, "Radiofrequency ablation for cancer: Definition," 2015.

3. R. C. Orth, M. J. Wallace, and M. D. Kuo, "C-arm cone-beam ct: General principles and technical considerations for use in interventional radiology," *Journal of Vascular and Interventional Radiology* **19**, pp. 814–820, June 2008.
4. F. Fani, E. Schena, P. Saccomandi, and S. Silvestri, "Ct-based thermometry: An overview," *International Journal of Hyperthermia* , June 2014.
5. F. P. M. Oliveira and J. M. R. S. Tavares, "Medical image registration: a review," *Computer Methods in Biomechanics and Biomedical Enginnering* , 2014.
6. D. L. G. Hill, P. G. Batchelor, M. Holden, and D. J. Hawkes, "Medical image registration," *Physics in Medicine and Biology* **46**(3), 2001.
7. S. Ourselin, A. Roche, G. Subsol, X. Pennec, and N. Ayache, "Reconstructing a 3d structure from serial histological sections," *Image and Vision Computing* , January 2001.
8. M. Modat, G. G. Ridgway, Z. A. Taylor, M. Lehmann, J. Barnes, N. C. Fox, D. J. Hawkes, and S. Ourselin, "Fast free-form deformation using graphics processing units," *Computer Methods and Programs in Biomedicine* , June 2010.
9. E. Durucan and T. Ebrahimi, "Change detection and background extraction by linear algebra," *Proceedings of the IEEE* **89**, pp. 1368–1381, Oct 2001.
10. D. K. Panda and S. Meher, "Video object segmentation based on adaptive background and wronskian change detection model," *2013 International Conference on Signal Processing and Communication* , 2013.
11. L.-M. Ang, *Visual Information Processing in Wireless Sensor Networks: Technology, Trends and Applications: Technology, Trends and Applications*, ch. 5, pp. 102–103. IGI Global, 2011.
12. B. Subudhi, S. Ghosh, and A. Ghosh, "Change detection for moving object segmentation with robust background construction under wronskian framework," *Machine Vision and Applications* **24**(4), pp. 795–809, 2013.
13. M. Rhudy, B. Bucci, J. Vipperman, J. Allanach, and B. Abraham, "Microphone array analysis methods using cross-correlations," *ASME Proceedings: Sound, Vibration and Design* , November 2009.
14. MathWorks, "Find connected components in raw image," 2015.
15. MathWorks, "Principal component analysis of raw data," 2015.
16. P. A. Yushkevich, J. Piven, H. Cody Hazlett, R. Gimpel Smith, S. Ho, J. C. Gee, and G. Gerig, "User-guided 3D active contour segmentation of anatomical structures: Significantly improved efficiency and reliability," *Neuroimage* **31**(3), pp. 1116–1128, 2006.
17. A. Fedorov, R. Beichel, J. Kalpathy-Cramer, J. Finet, J.-C. Fillion-Robin, S. Pujol, C. Bauer, D. Jennings, F. Fennessy, M. Sonka, J. Buatti, S. Aylward, J. Miller, S. Pieper, and R. Kikinis, "3d slicer as an image computing platform for the quantitative imaging network," *Magnetic Resonance Imaging* **30**, pp. 1323–41, 11 2012.
18. F. E. Boas and D. Fleischmann, "Evaluation of two iterative techniques for reducing metal artifacts in computed tomography," *Radiology* **259**(3), pp. 894–902, 2011.